Vertical Land Motion from present-day deglaciation in the wider Arctic

Carsten Ludwigsen[1], Shfaqat Abbas Khan[2], Ole Baltazar Andersen[3], and Ben Marzeion[4]

[1]Technical Univeresity of Denmark
[2]DTU Space
[3]DTU Space, National Space Institute
[4]University of Bremen

November 30, 2022

Abstract

Vertical land motion (VLM) of Earth's surface can aggravate or mitigate ongoing relative sea level change. The near-linear process of Glacial Isostatic Adjustment (GIA) is normally assumed to govern regional VLM. However, present-day deglaciation of primarily the Greenland Ice Sheet causes a significant non-linear elastic uplift of >1 mm yr -1 in most of the wider Arctic. The elastic VLM exceeds GIA at 14 of 42 Arctic GNSS-sites, including sites in non-glaciated areas in the North Sea region and along the east coast of North America. The combined elastic VLM + GIA model is consistent with measured VLM at three-fourth of the GNSS-sites (R=0.74), which outperforms a GIA-only model (R=0.60). Deviations from GNSS-measured VLM, are interpreted as estimates of local circumstances causing VLM. Future accelerated ice loss on Greenland, will increase the significance of elastic uplift for North America and Northern Europe and become important for coastal sea level projections.

Vertical Land Motion from present-day deglaciation in the wider Arctic

Carsten Ankjær Ludwigsen[1], Shfaqat Abbas Khan[1], Ben Marzeion[2] and Ole Baltazar Andersen[1]

[1]DTU Space, Technical University of Denmark
[2]Institute of Geography and MARUM – Center for Marine Environmental Sciences, University of Bremen, Germany

Key Points:

- Elastic VLM caused by present-day melt of Greenland causes significant uplift of coastlines in North America and Northern Europe.
- A VLM-model combining GIA and the elastic rebound from present-day ice loss yields good agreement with GNSS-stations in the wider Arctic.
- Residuals between GNSS and modeled VLM can quantify local circumstances causing VLM.

Corresponding author: Carsten Ankjær Ludwigsen, caanlu@space.dtu.dk

Abstract

Vertical land motion (VLM) of Earth's surface can aggravate or mitigate ongoing relative sea level change. The near-linear process of Glacial Isostatic Adjustment (GIA) is normally assumed to govern regional VLM. However, present-day deglaciation of primarily the Greenland Ice Sheet causes a significant non-linear elastic uplift of >1 mm yr^{-1} in most of the wider Arctic. The elastic VLM exceeds GIA at 14 of 42 Arctic GNSS-sites, including sites in non-glaciated areas in the North Sea region and along the east coast of North America. The combined elastic VLM + GIA model is consistent with measured VLM at three-fourth of the GNSS-sites (R=0.74), which outperforms a GIA-only model (R=0.60). Deviations from GNSS-measured VLM, are interpreted as estimates of local circumstances causing VLM. Future accelerated ice loss on Greenland, will increase the significance of elastic uplift for North America and Northern Europe and become important for coastal sea level projections.

Plain Language Summary

From 2003 to 2015, the Northern Hemisphere lost more than 6000 gigatonnes of ice, contributing with nearly 17 mm to the global mean sea level rise. Loss of land-based ice results in a vertical deformation of the Earths surface. An ongoing rebound or subsidence caused by the end of the last ice age is often assumed to govern the vertical deformation. But also present-day ice loss from Greenland and Arctic glaciers cause an immediate vertical deformation. By using an vertical deformation model, that includes both components, we can explain GPS-measured deformation in the entire Arctic. Our results show, that the present-day Arctic ice loss contribution to vertical deformation is an uplift in the order 0.5 to 1 mm/yr in a wider northern region. This exceeds the deformation caused by the disappearance of the last ice ages at many coastal regions, including the North Sea region and along the North American Atlantic coast. The present-day ice loss included in the VLM-model equals a global sea level rise of 1.4 mm/yr. This means that 30-80% of the sea level rise caused by Arctic ice loss is mitigated by an surface uplift caused by the same ice loss.

1 Introduction

The Arctic region is warming faster than any other region on Earth (Post et al., 2019). Deglaciation of Arctic land-based ice accounts for 70 % of the total barysteric contribution to sea level rise (Abram et al., 2019) and has over the last 3 decades accelerated the sea level rise with 0.035 mm yr^{-1} (Nerem et al., 2018) every year. From 2003 to 2015 the Greenland Ice Sheet and adjoining glaciers contributed in total with 1 cm of sea level rise while other Arctic glaciers contributed with 0.8 cm (Zemp et al., 2019).

Deglaciation of land ice is also changing the spatial pattern of sea level change. One effect of the redistribution of mass from ice to ocean is the gravitational change (Bamber & Riva, 2010; Hsu & Velicogna, 2017; Adhikari et al., 2019), and influx of freshwater changing the steric sea surface height (Ludwigsen & Andersen, 2020; Armitage et al., 2020). A more overlooked outcome of present-day deglaciation is vertical land motion (Riva et al., 2017). Vertical Land Motion (VLM) has to be taken into account and corrected for, when studying sea level change based on tide gauges (Watson et al., 2015; Wöppelmann & Marcos, 2016). Coastal uplift can mitigate the increasing risk of coastal flooding, while subsidence will aggravate the hazards caused by rising sea levels.

VLM is a composite of multiple ongoing processes, with the viscoelastic relaxation of the Earths surface since the ending of the last ice ages 21 kyr ago, also known as Glacial Isostatic Adjustment (GIA), being the most prominent component (Farrell & Clark, 1976; Tushingham & Peltier, 1991; Milne & Mitrovica, 1998; Peltier et al., 2015). In general, studies of coastal sea level change, only consider GIA (Church & White, 2011; Jevrejeva et al., 2014), while the elastic contribution is oftentimes ignored.

The physics of the immediate elastic surface response to the changing ice load is well known (Farrell, 1972), and can be used as a proxy for studying glacial ice mass balance (Khan et al., 2010, 2016). Locally, hydrology, tectonics and other seismic effects like earthquakes can be the single largest contribution to VLM (Klos et al., 2019) SLANGEN ref?.

While GIA is dominant in non-glaciated regions, GIA alone is insufficient to explain the measured VLM in the Arctic(Henry et al., 2012). We show, that the elastic VLM in the wider Arctic (roughly defined as the region above 50° latitude) caused by Arctic ice loss since 2003 is significant. The elastic VLM is for most of the region, including the North American coastlines and northern Europe, within the same magnitude as the corresponding barystatic sea level change.

2 Data and Method

Commonly, gravimetric ice mass change data from GRACE (The Gravity Recovery and Climate Experiment) is used to estimate surface loading (Adhikari et al., 2016; Riva et al., 2017; Frederikse et al., 2019). GRACE is convenient because it 'weighs' the Earth, and easily detects changes over time. The spatial signal wavelength of 300-500 km of GRACE is, however, insufficient to reproduce realistic elastic VLM-signals in the proximity of glaciers and ice sheets. Instead, we use mass balance data from Arctic glaciers and Greenland, to create an yearly ice-model with a 2 x 2 km spatial resolution from 2003-2015 (see section 2.1).

The ice-model surface loading is used as input for the REAR (Regional ElAstic Rebound calculator), (Melini et al., 2014, 2015) to make an elastic VLM-model with the same, high resolution (2 x 2 km). REAR is build on the sea level equation of Farrell and Clark (1976) and assumes a solid, non-rotating and isotropic earth. By combining GIA with the elastic VLM model, the VLM-model can be evaluated against GNSS measurements.

The calculated temporal average elastic VLM-rate from 2003-2015 is shown in figure 1. Yearly averaged mass balance changes of glaciers and the Greenland Ice Sheet (see section 2.1) from 2003-2015 are converted to elevation change assuming uniform ice density of 917 kg m^{-3} . The spatial resolution of the ice loading, used as input, and elastic VLM output is 2 x 2 km, allowing us to estimate VLM in the proximity of glaciers. The Love numbers used in REAR are defined with respect to Earth's centre of mass (CM-frame).

The ongoing vertical adjustment caused by the melting of the large ice caps 21 Kyr ago is defined as GIA. We use the GIA-model from Caron et al. (2018), which uses 128000 forward models of different 1D Earth rheologies and ice elevation histories to create the statistical best fit to long term GNSS observations and relative sea level records from tide gauges. Even though GIA decays over time, the deacceleration is negligible for short time periods and thus the GIA-rate is assumed to be constant.

Both the elastic VLM-model and GIA is defined globally. However, the scope of this study is the wider Arctic area. This doesn't mean that the elastic VLM is negligible outside this region, but the VLM-signal from present-day ice-loss created VLM will not be significant.

2.1 Ice Loading

The main component of the elastic VLM model is the loading model. The elevation change rate for the ice areas included in this study is shown in figure S1.1 in S1 (Supporting Information). We only consider Northern Hemisphere ice history, well aware that also Southern Hemisphere ice mass change my impact the region of this study (Riva et al., 2017). However, mass loss of the Southern Hemisphere is considerably smaller and specifically Antarctica is so far away, that it safely can be neglected.

2.1.1 Glaciers

Included in this study are all glaciers from the Randolph Glacier Inventory (RGI 6.0) (Pfeffer et al., 2014; RGI Consortium, 2017) from North America, Russia, Scandinavia (incl. Svalbard) and Iceland - in total more than 62.000 individual glaciers. The mass loss from the glaciers included covers 95 % of the registered glacial mass loss in the Northern Hemisphere and constitute 80% of the global glacial mass loss (Zemp et al., 2019).

Mass change estimates for each glacier is derived by updating the model of Marzeion et al. (2012). Direct mass balance observations (Zemp et al., 2019) are used for calibration and validation of the glacier model. The glacier model translates information about atmospheric conditions into glacier mass change, taking into account various feedbacks between glacier mass balance and glacier geometry.

Glacial mass balance is combined with a distribution function, D to create glacier-wide surface elevation changes. This ensures, that the lower parts of the glacier is thinning, while the top is experiencing an small elevation gain. This 'slope steepening' of glaciers is a characteristic pattern for glaciers in many regions (Nuth et al., 2010; Foresta et al., 2016; Ciracì et al., 2018) and is assumed to all glaciers included in this study (see Supporting Information S1 for more detail on the glacier model).

2.1.2 Greenland

The glacial ice history is combined with elevation change from the Greenland Ice Sheet and adjoining glaciers. We estimate the rate of ice volume change from 2003–2015 by using altimeter surveys from NASA's ATM flights (Krabill, 2011) during 2003–2015 supplemented with high-resolution Ice, Cloud and land Elevation Satellite (ICESat) data

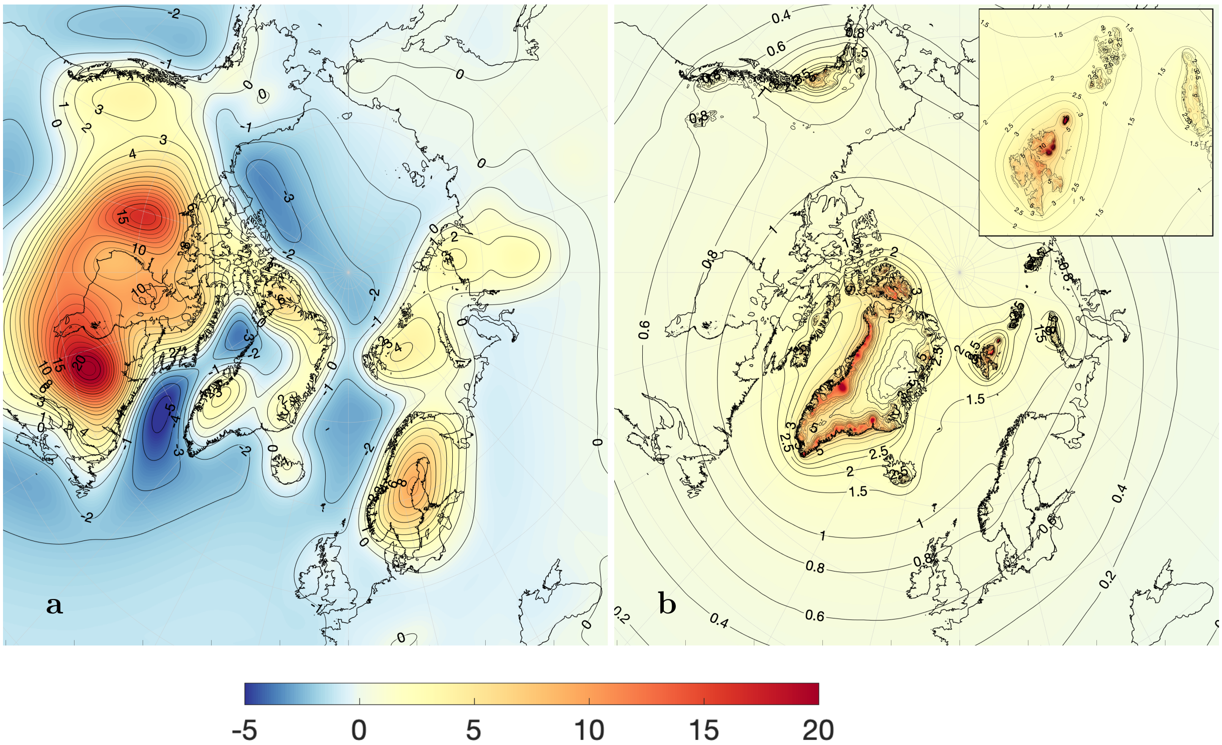

Figure 1. Average VLM rates (mm yr^{-1}) from 2003-2015 from Glacial Isostatic Adjustment (Caron et al., 2018) (**a**) and elastic rebound from contemporary land ice loss with enlargement of Svalbard (**b**).

(Zwally et al., 2011) during 2003–2009 and CryoSat-2 data during 2011-2015 (Helm et al., 2014). Our procedure for deriving ice surface elevation changes is described in detail by (Khan et al., 2013) and is similar to the method used by, e.g. Ewert et al. (2012); Smith et al. (2009) and Kjeldsen et al. (2013). We use the observed ice elevation change rates to interpolate (using collocation) ice thinning values onto the 2 x 2 km spatial grid. The volume loss rate is converted into a mass loss rate, taking firn compaction into account, as described by Kuipers Munneke et al. (2015).

2.2 GNSS data

Timeseries of vertical deformation and error estimates of 42 GNSS-sites are from the sixth release of the consortium lead by University of La Rochelle (ULR-6) (Santamaría-Gómez et al., 2017) (detailed map and timeseries of all glaciers are shown in S2 figure S2.1 and S3 figure S3.1). ULR-6 includes more than 80 GNSS-sites located in the area of interest, but we only select GNSS-sites with data in at least 120 of 156 months from 2003 to 2015 and where no known human impact is present. Furthermore, only one GNSS-sites is selected based on the timeseries with the lowest standard deviation, when multiple GNSS-sites are located within 50 km of each other. The annual average is calculated for each GNSS-site and gaps are filled by assuming linearity. The trend estimates are calculated from the original time-series with outliers of more than $> 2\sigma$ removed.

3 Evaluating the VLM model

In figure 2, the VLM-model from 2003 to 2015, which is the sum of GIA and the modeled elastic VLM from figure 1, is shown together with VLM-rates from the GNSS sites described in section 2.2.

The model is dominated by the pattern of the GIA-model, with rates above 20 mm yr^{-1} east of the Hudson Bay and another local maximum of over 15 mm yr^{-1} in northwest Canada. The elastic rebound is evident, particular in Greenland with rates exceeding 10 mm yr^{-1}. Large areas around Svalbard and Alaska have modeled elastic VLM-rates of more than 6 mm yr^{-1}.

The largest rates of vertical deformations are areas dominated by elastic VLM. Jakobshavn Issbræ, north of Kangerlussuaq (KELY), has rates above 40 mm yr^{-1}. Similarly the area of Austfonna glacier on Svalbard has rates above 30 mm yr^{-1}. The largest depression zones are over the ocean, with the Beaufort Sea and Labrador Sea having rates below -2 mm yr^{-1} and the Norwegian Sea with rates below -1.5 mm yr^{-1}. Subsiding coastal areas are found in North America, where Nova Scotia and most of the US east- and west-coast subsides with more than -1 mm yr^{-1}, while smaller subsidence (-0.5 - 0.0 mm yr^{-1}) is found in Northern Europe along the North Sea and Atlantic coastlines.

Figure 3 shows, that for large areas of the Arctic, the elastic VLM can be attributed with at least 30% from the VLM-signal. When GIA is small or zero, the elastic VLM is determining the vertical deformation. This is true for large areas in east Siberia and a band following around the North American east and west coast, as well as the northern part of the British Isles and the southern parts of Denmark and the Baltic Sea coast line.

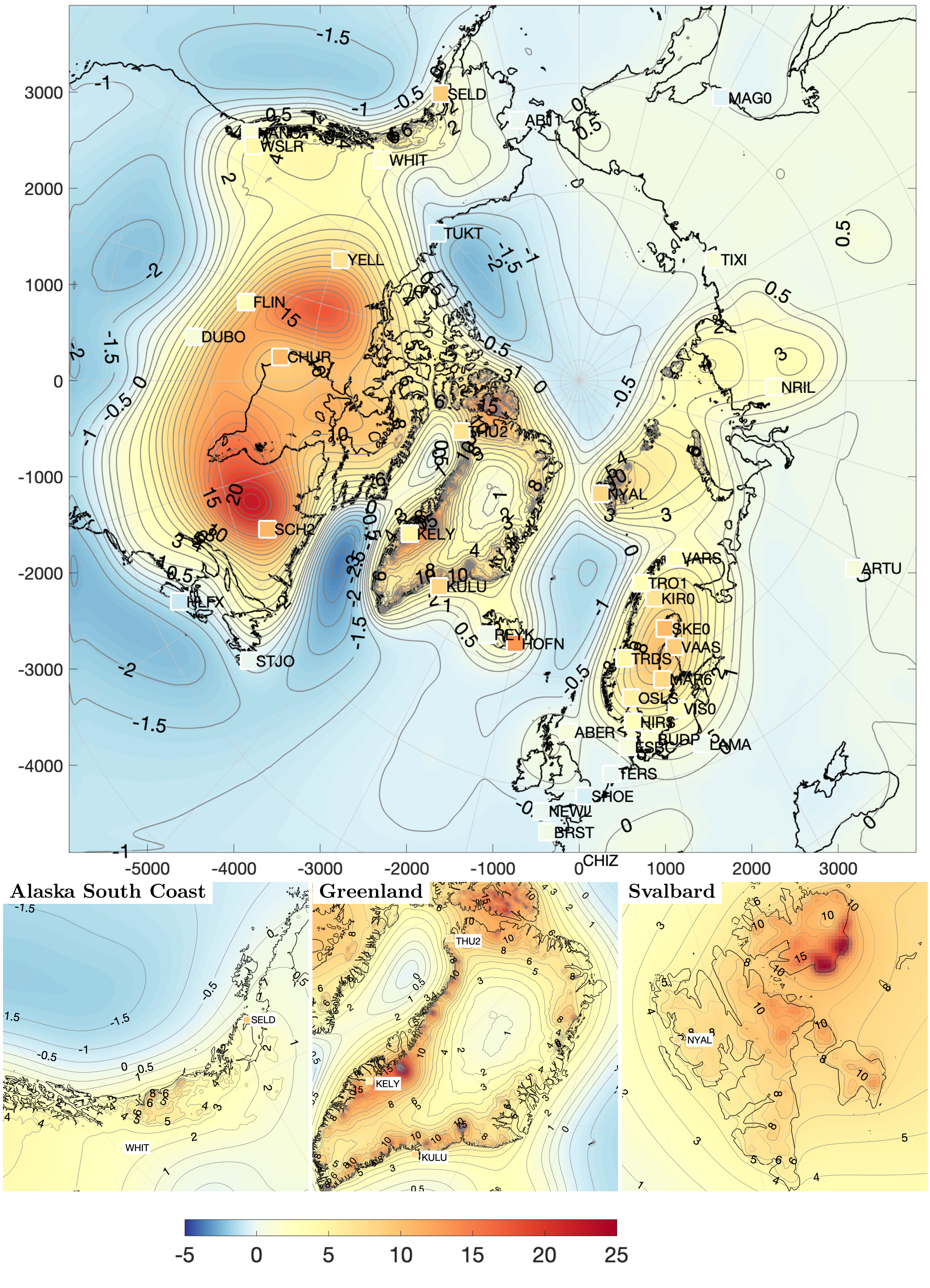

Figure 2. Average VLM-rates (mm yr^{-1}) from 2003-2015 from the VLM-model (Glacial Isostatic Adjustment + elastic VLM). The color of the squares represent the GNSS measured average VLM-rate for the same period. For clarification Alaska South Coast, Greenland and Svalbard are enlarged below.

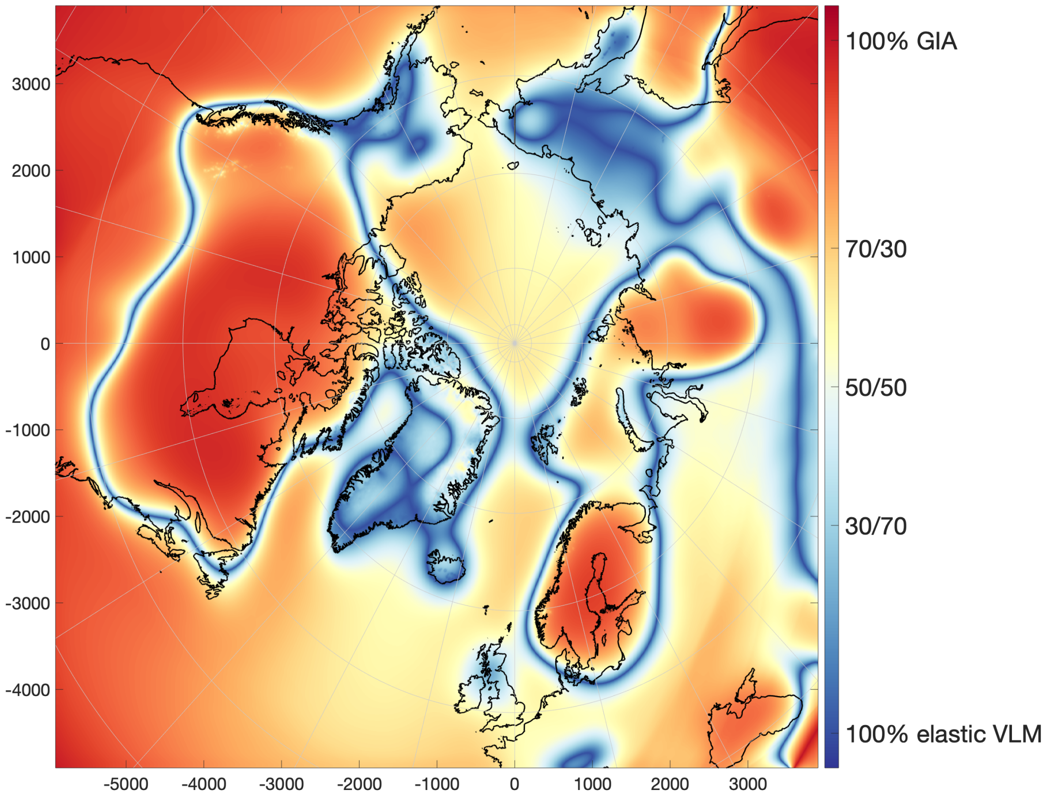

Figure 3. The share of GIA-rate and elastic VLM-rate from the total absolute VLM-rate (in absolute terms) in percentage. Red colors indicate areas where GIA dominates VLM while blue colors indicate where the elastic VLM is larger.

While the general uplift pattern from the VLM-model is reflected in the GNSS rates, residuals between GNSS VLM and the VLM model are evident, in particular close to glaciers. Figure 4 displays the difference between the VLM-model and the GNSS-measured VLM. The two largest differences are found in Seldovia, Alaska (SELD) and Hoefn, Iceland (HOFN). For Seldovia a large earthquake in 1964 is still causing displacement (Cohen & Freymueller, 2001), where on Iceland particular soft mantle structures creates larger uplift rates than predicted with the isotropic VLM-model (Fleming et al., 2007; Sørensen et al., 2017). The difference indicates the scale that extraordinary subsurface properties or post-seismic activities can have locally. More detailed information on local causes explaining the residuals in figure 4 are described in S2, table S2.1 and figure S3.1.

Some uncertainty is connected with the choice of GIA-model, for instance, the ICE6G-model from Peltier et al. (2015) has in other studies shown to provide a better fit to GNSS-sites in North America (Schumacher et al., 2018; Frederikse et al., 2019), where it seems that the Caron2018-model overestimates GIA slightly. In the early stages of this study, the Caron 2018 model provided the on average best fit to GNSS data compared to other GIA-models.

Figure 4 shows that the VLM-model including uncertainty is within the range of GNSS-measured VLM for 33 of the 42 GNSS locations. The correlation between measured VLM and GIA is 0.61, which improves to 0.74 when adding the elastic VLM to GIA (i.e. the VLM-model). The mean absolute error (MAE) of the 42 GNSS-sites is 1.54 mm yr^{-1}, which is 0.55 mm yr^{-1} better than a GIA-only model (2.09 mm yr^{-1}). If we don't consider sites located in glaciated areas (i.e. SELD, WHIT, THU2, KELY, KULU, REYK, HOFN, NYAL), then MAE becomes 0.89 mm yr^{-1} for the VLM-model which is significantly lower than 1.12 mm yr^{-1} for GIA-only.

When comparing to the associated barysteric sea level change of $\sim$1.4 mm yr^{-1} (i.e. the ice loss created global average sea level change) is the elastic VLM significantly mitigating the sea level change at most GNSS-sites in this study (see figure 4)

The elastic VLM-rate is not linear, but unlike GIA, varies from year to year in accordance with the annual ice loss, as the elastic response is instant. This is in particular visible close to the ice loss, where the signal is largest and GNSS-measured VLM can be used as a proxy for the surrounding ice loss. Figure 5 shows how closely the VLM-model non linear follows the GNSS signal in Thule (THU2) in northern Greenland.

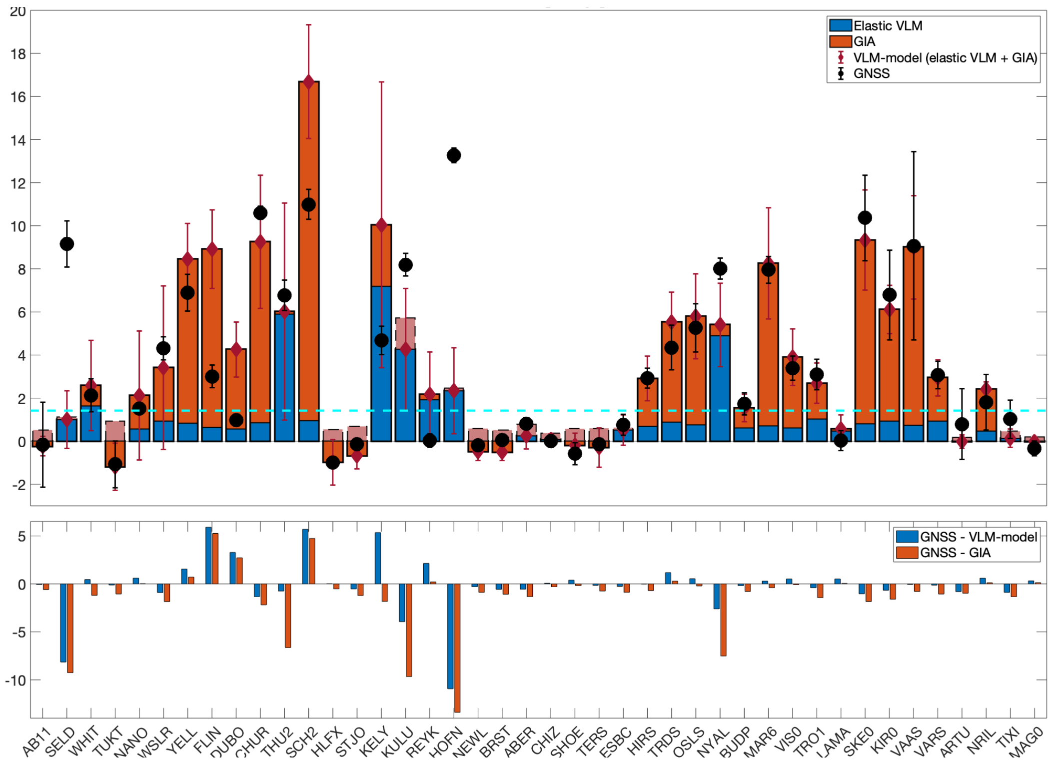

Figure 4. Top: 2003-2015 average VLM change [mm yr^{-1}] from the elastic VLM model (blue) and GIA (red) at 42 GNSS-sites shown in figure 2 and Supporting Information S2.1 ordered from most west (left) to most east (right). The dotted-cyan line indicates the average barysteric sea level rise ($\sim$ 1.4 mm yr^{-1}) from the ice loss included in this study. The total modeled VLM and the error is shown with red error bars and the GNSS measured VLM is shown with black error bars. The lighter red indicates where GIA is negative and hence overlaps the positive elastic VLM. Bottom: The residuals between GNSS-measured VLM and the VLM-model (blue) and GIA (red). The average of the absolute residuals (equivalent to Mean Absolute Error) is 1.54 mm yr^{-1} and 2.09 mm yr^{-1} respectively. All numbers for this figure are given in Supporting Information table S2.1.

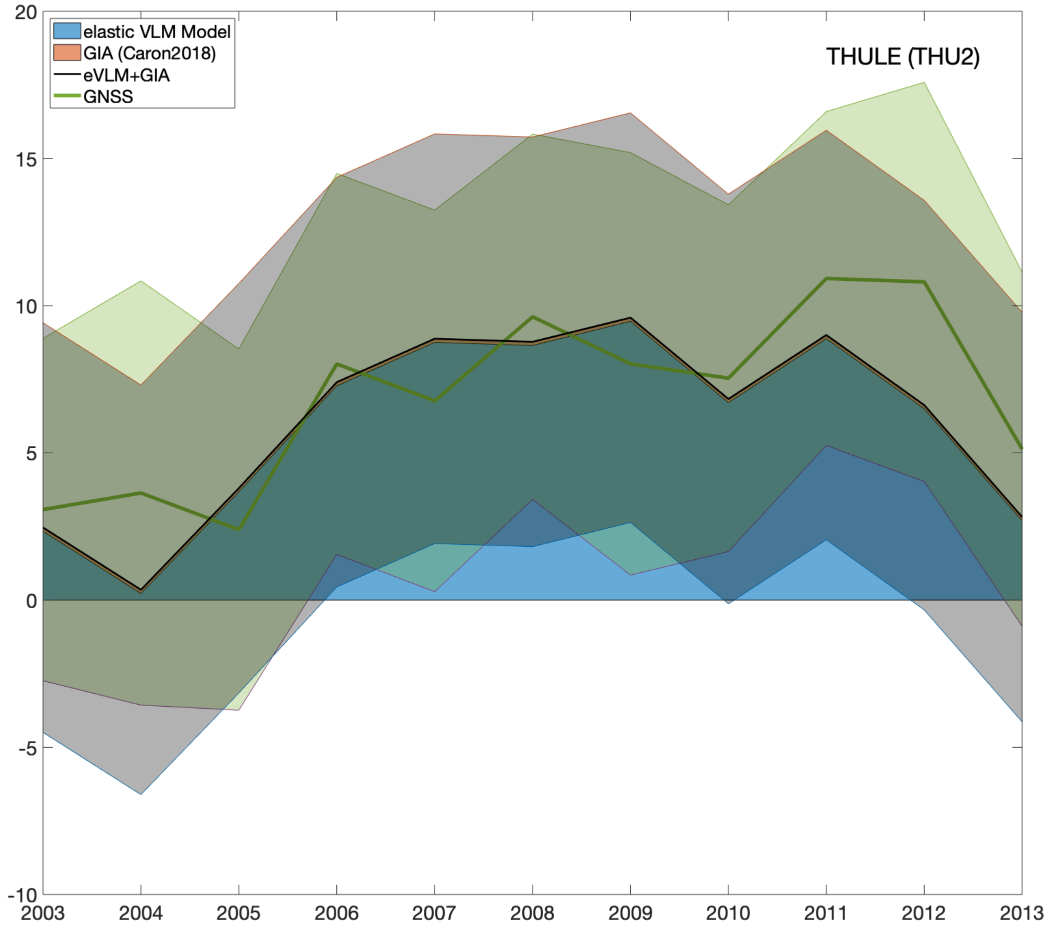

Figure 5. Yearly displacement (mm) for Thule (Northeast Greenland) from 2003 to 2013, measured by GNSS (green line - shaded green area is 1σ)) and from the VLM-model (black line - shaded grey area is 1σ). The elastic VLM is represented by the blue area and GIA by the orange area, which in this case is small.

4 Discussion and Conclusion

Vertical Land Motion in the wider Arctic originates from many ongoing processes, with GIA and elastic VLM being the most important ones on regional to global scales. Even though this study is limited to an wider area around the Arctic, the VLM caused by changing cryosphere is a global effect (Riva et al., 2017; Kleinherenbrink et al., 2018; Frederikse et al., 2019).

By combining prehistoric (GIA) and present-day land ice change (elastic VLM), the VLM-model gives a realistic estimate on how the solid earth in the Arctic vertically deforms. By evaluating 42 selected GNSS-sites with a combined VLM-model, we find that the measured uplift by GNSS can be explained by either prehistoric or present-day land ice changes. For 33 of the GNSS-sites, the residual between GNSS measured VLM and the VLM-model is smaller than the associated errors.

The 2 x 2-km spatial resolution of the VLM-model is much higher than similar products from gravimetric satellite observations from GRACE (Adhikari et al., 2019). The spatial resolution improves the accuracy of VLM-predictions in glaciated regions, as local patterns of elastic deformation dominate the regional averages seen by GRACE (Frederikse et al., 2019). The VLM-model to GNSS comparison also indicates, that the VLM-model is inadequate in some regions due to local causes not covered by the VLM-model showing the scale of subsurface properties, past seismic activity or 19-20th century ice-loss (as seen on Svalbard (Mémin et al., 2014; Rajner, 2018)). A more detailed explanation of possible causes for differences between GNSS and the VLM is described in S2.

In non-glaciated areas, GNSS measurements have generally good agreement with the VLM-model. The contour lines in figure 1 shows that the elastic uplift is centered around Greenland, except close to other glaciated regions (e.g. Alaska and Svalbard), even though the total mass loss of the Arctic glaciers is comparable with the Greenland ice mass loss. Hence, the elastic uplift caused by Greenland ice melt is significant in the entire wider Arctic including the coastlines in Northern Europe and along the North American Atlantic.

Riva et al. (2017) showed, that the elastic uplift caused by Greenland eventually becomes negative in the Southern Hemisphere, which also means that Antarctica has a similar effect on the Northern Hemisphere. Antarctica experienced about half of the ice loss of Greenland during 2003-2015. However, we found that the Antarctic elastic VLM contribution is insignificant compared to that of the Northern Hemisphere and has uniform pattern for the region of this study. With potential future rapid ice loss (a.o. Edwards et al. (2019)), VLM caused by Antarctic ice loss will gain significance in the far field and hence be important to include for future coastal sea level projections in the Northern Hemisphere.

Acknowledgments

Thanks to Danielle Melini (Melini et al., 2014), for creating the REAR-code, which has been very helpful for creating the VLM-model. Greatly appreciated is the work of A. Caron (Caron et al., 2018) on the GIA-model, which is available from the NASA JPL website `https://vesl.jpl.nasa.gov/solid-earth/gia/`. The elastic VLM-model is freely available at `ftp.space.dtu.dk/pub/DTU20/VLM`. The project is partly funded by the EU-INTAROS project (Grant agreement 727890) and the ESA-Climate Change Initiative Sea level budget closure (Expro RFP/3-14679/16/I-NB).

References

Abram, N., Adler, C., Bindoff, N., Cheng, L., Cheong, S.-M., Cheung, W., … Zhai, P. (2019, 09). Summary for policymakers. in: Ipcc special report on the ocean

and cryosphere in a changing climate..
Adhikari, S., Ivins, E. R., Frederikse, T., Landerer, F. W., & Caron, L. (2019). Sea-level fingerprints emergent from grace mission data. *Earth System Science Data*, *11*(2), 629–646. Retrieved from https://www.earth-syst-sci-data.net/11/629/2019/ doi: 10.5194/essd-11-629-2019
Adhikari, S., Ivins, E. R., & Larour, E. (2016). Issm-sesaw v1.0: mesh-based computation of gravitationally consistent sea-level and geodetic signatures caused by cryosphere and climate driven mass change. *Geoscientific Model Development*, *9*(3), 1087–1109. Retrieved from https://www.geosci-model-dev.net/9/1087/2016/ doi: 10.5194/gmd-9-1087-2016
Armitage, T. W. K., Manucharyan, G. E., Petty, A. A., Kwok, R., & Thompson, A. F. (2020). Enhanced eddy activity in the beaufort gyre in response to sea ice loss. *Nature Communications*, *11*(1), 761. Retrieved from https://doi.org/10.1038/s41467-020-14449-z doi: 10.1038/s41467-020-14449-z
Bamber, J., & Riva, R. (2010). The sea level fingerprint of recent ice mass fluxes. *The Cryosphere*, *4*(4), 621–627. Retrieved from https://www.the-cryosphere.net/4/621/2010/ doi: 10.5194/tc-4-621-2010
Caron, L., Ivins, E. R., Larour, E., Adhikari, S., Nilsson, J., & Blewitt, G. (2018). Gia model statistics for grace hydrology, cryosphere, and ocean science. *Geophysical Research Letters*, *45*(5), 2203-2212. Retrieved from https://agupubs.onlinelibrary.wiley.com/doi/abs/10.1002/2017GL076644 doi: 10.1002/2017GL076644
Church, J., & White, N. (2011). Sea-level rise from the late 19th to the early 21st century. *Surveys in Geophysics*, *32*(4-5), 585-602. Retrieved from https://www.scopus.com/inward/record.uri?eid=2-s2.0-80053195533&doi=10.1007%2fs10712-011-9119-1&partnerID=40&md5=a6a2b9bb53f622e9bf4b3266a27d54f0 (cited By 737) doi: 10.1007/s10712-011-9119-1
Ciracì, E., Velicogna, I., & Sutterley, T. C. (2018). Mass balance of novaya zemlya archipelago, russian high arctic, using time-variable gravity from grace and altimetry data from icesat and cryosat-2. *Remote Sensing*, *10*(11). Retrieved from https://www.mdpi.com/2072-4292/10/11/1817 doi: 10.3390/rs10111817
Cohen, S. C., & Freymueller, J. T. (2001). Crustal uplift in the south central alaska subduction zone: New analysis and interpretation of tide gauge observations. *Journal of Geophysical Research: Solid Earth*, *106*(B6), 11259-11270. Retrieved from https://agupubs.onlinelibrary.wiley.com/doi/abs/10.1029/2000JB900419 doi: 10.1029/2000JB900419
Edwards, T., Brandon, M., Durand, G., Edwards, N., Golledge, N., Holden, P., ... Wernecke, A. (2019, 02). Revisiting antarctic ice loss due to marine ice-cliff instability. *Nature*, *566*, 58-64. doi: 10.1038/s41586-019-0901-4
Ewert, H., Groh, A., & Dietrich, R. (2012, September). Volume and mass changes of the Greenland ice sheet inferred from ICESat and GRACE. *Journal of Geodynamics*, *59-60*, 111-123. doi: 10.1016/j.jog.2011.06.003
Farrell, W. E. (1972). Deformation of the earth by surface loads. *Reviews of Geophysics*, *10*(3), 761-797. Retrieved from https://agupubs.onlinelibrary.wiley.com/doi/abs/10.1029/RG010i003p00761 doi: 10.1029/RG010i003p00761
Farrell, W. E., & Clark, J. A. (1976). On postglacial sea level. *Geophysical Journal of the Royal Astronomical Society*, *46*(3), 647-667. Retrieved from https://onlinelibrary.wiley.com/doi/abs/10.1111/j.1365-246X.1976.tb01252.x doi: 10.1111/j.1365-246X.1976.tb01252.x
Fleming, K., Martinec, Z., & Wolf, D. (2007, 01). Glacial-isostatic adjustment and the viscosity structure underlying the vatnajökull ice cap, iceland. *Pure and Applied Geophysics*, *164*, 751-768. doi: 10.1007/s00024-007-0187-6

Foresta, L., Gourmelen, N., Pálsson, F., Nienow, P., Björnsson, H., & Shepherd, A. (2016). Surface elevation change and mass balance of icelandic ice caps derived from swath mode cryosat-2 altimetry. *Geophysical Research Letters*, *43*(23), 12,138-12,145. Retrieved from https://agupubs.onlinelibrary.wiley.com/doi/abs/10.1002/2016GL071485 doi: 10.1002/2016GL071485

Frederikse, T., Landerer, F. W., & Caron, L. (2019). The imprints of contemporary mass redistribution on local sea level and vertical land motion observations. *Solid Earth*, *10*(6), 1971–1987. Retrieved from https://www.solid-earth.net/10/1971/2019/ doi: 10.5194/se-10-1971-2019

Helm, V., Humbert, A., & Miller, H. (2014). Elevation and elevation change of greenland and antarctica derived from cryosat-2. *The Cryosphere*, *8*(4), 1539–1559. Retrieved from https://www.the-cryosphere.net/8/1539/2014/ doi: 10.5194/tc-8-1539-2014

Henry, O., Prandi, P., Llovel, W., Cazenave, A., Jevrejeva, S., Stammer, D., ... Koldunov, N. (2012). Tide gauge-based sea level variations since 1950 along the norwegian and russian coasts of the arctic ocean: Contribution of the steric and mass components. *Journal of Geophysical Research: Oceans*, *117*(C6). Retrieved from https://agupubs.onlinelibrary.wiley.com/doi/abs/10.1029/2011JC007706 doi: 10.1029/2011JC007706

Hsu, C.-W., & Velicogna, I. (2017). Detection of sea level fingerprints derived from grace gravity data. *Geophysical Research Letters*, *44*(17), 8953-8961. Retrieved from https://agupubs.onlinelibrary.wiley.com/doi/abs/10.1002/2017GL074070 doi: 10.1002/2017GL074070

Jevrejeva, S., Moore, J., Grinsted, A., Matthews, A., & Spada, G. (2014). Trends and acceleration in global and regional sea levels since 1807. *Global and Planetary Change*, *113*, 11-22. Retrieved from https://www.scopus.com/inward/record.uri?eid=2-s2.0-84890953576&doi=10.1016%2fj.gloplacha.2013.12.004&partnerID=40&md5=67194675f8fc061f1bb025a9fb67361f (cited By 85) doi: 10.1016/j.gloplacha.2013.12.004

Khan, S. A., Kjær, K. H., Korsgaard, N. J., Wahr, J., Joughin, I. R., Timm, L. H., ... Babonis, G. (2013). Recurring dynamically induced thinning during 1985 to 2010 on upernavik isstrøm, west greenland. *Journal of Geophysical Research: Earth Surface*, *118*(1), 111-121. Retrieved from https://agupubs.onlinelibrary.wiley.com/doi/abs/10.1029/2012JF002481 doi: 10.1029/2012JF002481

Khan, S. A., Liu, L., Wahr, J., Howat, I., Joughin, I., Dam, T. v., & Fleming, K. (2010, 9). GPS measurements of crustal uplift near Jakobshavn Isbræ due to glacial ice mass loss. *Journal of Geophysical Research: Solid Earth (1978–2012)*, *115*(B9). Retrieved from https://doi.org/10.1029/2010JB007490 doi: 10.1029/2010JB007490

Khan, S. A., Sasgen, I., Bevis, M., van Dam, T., Bamber, J. L., Wahr, J., ... Munneke, P. K. (2016). Geodetic measurements reveal similarities between post–last glacial maximum and present-day mass loss from the greenland ice sheet. *Science Advances*, *2*(9). Retrieved from https://advances.sciencemag.org/content/2/9/e1600931 doi: 10.1126/sciadv.1600931

Kjeldsen, K. K., Khan, S. A., Wahr, J., Korsgaard, N. J., Kjær, K. H., Bjørk, A. A., ... van Angelen, J. H. (2013). Improved ice loss estimate of the northwestern greenland ice sheet. *Journal of Geophysical Research: Solid Earth*, *118*(2), 698-708. Retrieved from https://agupubs.onlinelibrary.wiley.com/doi/abs/10.1029/2012JB009684 doi: 10.1029/2012JB009684

Kleinherenbrink, M., Riva, R., & Frederikse, T. (2018). A comparison of methods to estimate vertical land motion trends from gnss and altimetry at tide gauge stations. *Ocean Science*, *14*(2), 187-204. Retrieved from https://www.scopus.com/inward/record.uri?eid=2-s2.0-85044121271&doi=10.5194%2fos-14-187-2018&partnerID=40&md5=dbe85241ab9f3400fe3f655c42918079 (cited

By 6) doi: 10.5194/os-14-187-2018

Klos, A., Kusche, J., Fenoglio-Marc, L., Bos, M. S., & Bogusz, J. (2019, Jul 24). Introducing a vertical land motion model for improving estimates of sea level rates derived from tide gauge records affected by earthquakes. *GPS Solutions*, *23*(4), 102. Retrieved from https://doi.org/10.1007/s10291-019-0896-1 doi: 10.1007/s10291-019-0896-1

Krabill, W. B. (2011). *Icebridge atm l2 icessn elevation, slope, and roughness, [1993-2012].* (Boulder, Colorado: NASA Distributed Active Archive Center at the National Snow and Ice Data Center) doi: 10.5067/ICESAT/GLAS/DATA225

Kuipers Munneke, P., Ligtenberg, S. R. M., Noël, B. P. Y., Howat, I. M., Box, J. E., Mosley-Thompson, E., ... van den Broeke, M. R. (2015). Elevation change of the greenland ice sheet due to surface mass balance and firn processes, 1960-2014. *The Cryosphere*, *9*(6), 2009–2025. Retrieved from https://www.the-cryosphere.net/9/2009/2015/ doi: 10.5194/tc-9-2009-2015

Ludwigsen, C. A., & Andersen, O. B. (2020). Contributions to arctic sea level from 2003 to 2015. *Advances in Space Research*. Retrieved from http://www.sciencedirect.com/science/article/pii/S0273117719309275 doi: https://doi.org/10.1016/j.asr.2019.12.027

Marzeion, B., Jarosch, A. H., & Hofer, M. (2012). Past and future sea-level change from the surface mass balance of glaciers. *The Cryosphere*, *6*(6), 1295–1322. Retrieved from https://www.the-cryosphere.net/6/1295/2012/ doi: 10.5194/tc-6-1295-2012

Melini, D., Gegout, P., King, M., Marzeion, B., & Spada, G. (2015, 08). On the rebound: Modeling earth's ever-changing shape. *Eos Transactions American Geophysical Union*, *96*. doi: 10.1029/2015EO033387

Melini, D., Spada, G., Gegout, P., & King, M. (2014, 01). *Rear - a regional elastic rebound calculator. user manual for version 1.0.* Retrieved from http://hpc.rm.ingv.it/rear

Milne, G. A., & Mitrovica, J. X. (1998, 04). Postglacial sea-level change on a rotating Earth. *Geophysical Journal International*, *133*(1), 1-19. Retrieved from https://doi.org/10.1046/j.1365-246X.1998.1331455.x doi: 10.1046/j.1365-246X.1998.1331455.x

Nerem, R. S., Beckley, B. D., Fasullo, J. T., Hamlington, B. D., Masters, D., & Mitchum, G. T. (2018). Climate-change–driven accelerated sea-level rise detected in the altimeter era. *Proceedings of the National Academy of Sciences*, *115*(9), 2022–2025. Retrieved from https://www.pnas.org/content/115/9/2022 doi: 10.1073/pnas.1717312115

Nuth, C., Moholdt, G., Kohler, J., Hagen, J. O., & Kääb, A. (2010). Svalbard glacier elevation changes and contribution to sea level rise. *Journal of Geophysical Research: Earth Surface*, *115*(F1). Retrieved from https://agupubs.onlinelibrary.wiley.com/doi/abs/10.1029/2008JF001223 doi: 10.1029/2008JF001223

Peltier, W., Argus, D., & Drummond, R. (2015). Space geodesy constrains ice age terminal deglaciation: The global ice-6g-c (vm5a) model. *Journal of Geophysical Research: Solid Earth*, *120*(1), 450-487. Retrieved from https://www.scopus.com/inward/record.uri?eid=2-s2.0-85027948080&doi=10.1002%2f2014JB011176&partnerID=40&md5=29a7ce38c5cf3872d2276981d2f6b34f (cited By 326) doi: 10.1002/2014JB011176

Pfeffer, W. T., Arendt, A. A., Bliss, A., Bolch, T., Cogley, J. G., Gardner, A. S., ... et al. (2014). The randolph glacier inventory: a globally complete inventory of glaciers. *Journal of Glaciology*, *60*(221), 537–552. doi: 10.3189/2014JoG13J176

Post, E., Alley, R. B., Christensen, T. R., Macias-Fauria, M., Forbes, B. C., Gooseff, M. N., ... Wang, M. (2019). The polar regions in a 2c warmer world. *Science Advances*, *5*(12). Retrieved from https://advances.sciencemag.org/

content/5/12/eaaw9883 doi: 10.1126/sciadv.aaw9883
RGI Consortium. (2017). *Randolph Glacier Inventory – A Dataset of Global Glacier Outlines: Version 6.0: Technical Report.* (https://doi.org/10.7265/N5-RGI-60)

Riva, E., Frederikse, T., King, A., Marzeion, B., & Van Den Broeke, R. (2017). Brief communication: The global signature of post-1900 land ice wastage on vertical land motion. *Cryosphere*, *11*(3), 1327-1332. Retrieved from https://www.scopus.com/inward/record.uri?eid=2-s2.0-85020484420&doi=10.5194%2ftc-11-1327-2017&partnerID=40&md5=077251aec38900cef0ec0ecdd2b1eded (cited By 11) doi: 10.5194/tc-11-1327-2017

Santamaría-Gómez, A., Gravelle, M., Dangendorf, S., Marcos, M., Spada, G., & Wöppelmann, G. (2017). Uncertainty of the 20th century sea-level rise due to vertical land motion errors. *Earth and Planetary Science Letters*, *473*, 24 - 32. Retrieved from http://www.sciencedirect.com/science/article/pii/S0012821X17303060 doi: https://doi.org/10.1016/j.epsl.2017.05.038

Schumacher, M., King, M., Rougier, J., Sha, Z., Khan, S., & Bamber, J. (2018). A new global gps data set for testing and improving modelled gia uplift rates. *Geophysical Journal International*, *214*(3), 2164-2176. Retrieved from https://www.scopus.com/inward/record.uri?eid=2-s2.0-85050475763&doi=10.1093%2fgji%2fggy235&partnerID=40&md5=0b6d3ed0cdf0208346d1d8bb4bed2c40 (cited By 5) doi: 10.1093/gji/ggy235

Smith, B. E., Fricker, H. A., Joughin, I. R., & Tulaczyk, S. (2009). An inventory of active subglacial lakes in antarctica detected by icesat (2003–2008). *Journal of Glaciology*, *55*(192), 573–595. doi: 10.3189/002214309789470879

Sørensen, L. S., Jarosch, A. H., Adalgeirsdóttir, G., Barletta, V. R., Forsberg, R., Pálsson, F., … Jóhannesson, T. (2017, 01). The effect of signal leakage and glacial isostatic rebound on GRACE-derived ice mass changes in Iceland. *Geophysical Journal International*, *209*(1), 226-233. Retrieved from https://doi.org/10.1093/gji/ggx008 doi: 10.1093/gji/ggx008

Tushingham, A. M., & Peltier, W. R. (1991). Ice-3g: A new global model of late pleistocene deglaciation based upon geophysical predictions of post-glacial relative sea level change. *Journal of Geophysical Research: Solid Earth*, *96*(B3), 4497-4523. Retrieved from https://agupubs.onlinelibrary.wiley.com/doi/abs/10.1029/90JB01583 doi: 10.1029/90JB01583

Watson, C. S., White, N. J., Church, J. A., King, M. A., Burgette, R. J., & Legresy, B. (2015, JUN). Unabated global mean sea-level rise over the satellite altimeter era. *NATURE CLIMATE CHANGE*, *5*(6), 565+.

Wöppelmann, G., & Marcos, M. (2016). Vertical land motion as a key to understanding sea level change and variability. *Reviews of Geophysics*, *54*(1), 64-92. Retrieved from https://agupubs.onlinelibrary.wiley.com/doi/abs/10.1002/2015RG000502 doi: 10.1002/2015RG000502

Zemp, M., Huss, M., Thibert, E., Eckert, N., McNabb, R., Huber, J., … Cogley, J. G. (2019). Global glacier mass changes and their contributions to sea-level rise from 1961 to 2016. *Nature*, *568*(7752), 382-386. doi: 10.1038/s41586-019-1071-0

Zwally, H. J., Schutz, R., Bentley, C., Bufton, J., Herring, T., Minster, J., … Thomas, R. (2011). *Glas/icesat l2 antarctic and greenland ice sheet altimetry data v031.* (Boulder, Colorado: NASA Distributed Active Archive Center at the National Snow and Ice Data Center) doi: 10.5067/CPRXXK3F39RV

References of Supporting Information:

Caron, L., Ivins, E. R., Larour, E., Adhikari, S., Nilsson, J., & Blewitt, G. (2018). Gia model statistics for grace hydrology, cryosphere, and ocean science. *Geo-*

physical Research Letters, *45*(5), 2203-2212. Retrieved from https://agupubs.onlinelibrary.wiley.com/doi/abs/10.1002/2017GL076644 doi: 10.1002/2017GL076644

Cohen, S. C., & Freymueller, J. T. (2001). Crustal uplift in the south central alaska subduction zone: New analysis and interpretation of tide gauge observations. *Journal of Geophysical Research: Solid Earth*, *106*(B6), 11259-11270. Retrieved from https://agupubs.onlinelibrary.wiley.com/doi/abs/10.1029/2000JB900419 doi: 10.1029/2000JB900419

Fleming, K., Martinec, Z., & Wolf, D. (2007, 01). Glacial-isostatic adjustment and the viscosity structure underlying the vatnajökull ice cap, iceland. *Pure and Applied Geophysics*, *164*, 751-768. doi: 10.1007/s00024-007-0187-6

Frederikse, T., Landerer, F. W., & Caron, L. (2019). The imprints of contemporary mass redistribution on local sea level and vertical land motion observations. *Solid Earth*, *10*(6), 1971–1987. Retrieved from https://www.solid-earth.net/10/1971/2019/ doi: 10.5194/se-10-1971-2019

Grove, J. (2001, 01). The initiation of the "little ice age" in regions round the north atlantic. *Climatic Change*, *48*, 53-82. doi: 10.1023/A:1005662822136

Hu, Y., & Freymueller, J. T. (2019). Geodetic observations of time-variable glacial isostatic adjustment in southeast alaska and its implications for earth rheology. *Journal of Geophysical Research: Solid Earth*, *124*(9), 9870-9889. Retrieved from https://agupubs.onlinelibrary.wiley.com/doi/abs/10.1029/2018JB017028 doi: 10.1029/2018JB017028

Kierulf, H. P., Plag, H.-P., & Kohler, J. (2009, 10). Surface deformation induced by present-day ice melting in Svalbard. *Geophysical Journal International*, *179*(1), 1-13. Retrieved from https://doi.org/10.1111/j.1365-246X.2009.04322.x doi: 10.1111/j.1365-246X.2009.04322.x

Larsen, C. F., Motyka, R. J., Freymueller, J. T., Echelmeyer, K. A., & Ivins, E. R. (2005). Rapid viscoelastic uplift in southeast alaska caused by post-little ice age glacial retreat. *Earth and Planetary Science Letters*, *237*(3), 548 - 560. Retrieved from http://www.sciencedirect.com/science/article/pii/S0012821X05004152 doi: https://doi.org/10.1016/j.epsl.2005.06.032

Mémin, A., Spada, G., Boy, J.-P., Rogister, Y., & Hinderer, J. (2014, 05). Decadal geodetic variations in Ny-Ålesund (Svalbard): role of past and present ice-mass changes . *Geophysical Journal International*, *198*(1), 285-297. Retrieved from https://doi.org/10.1093/gji/ggu134 doi: 10.1093/gji/ggu134

Peltier, W., Argus, D., & Drummond, R. (2015). Space geodesy constrains ice age terminal deglaciation: The global ice-6g-c (vm5a) model. *Journal of Geophysical Research: Solid Earth*, *120*(1), 450-487. Retrieved from https://www.scopus.com/inward/record.uri?eid=2-s2.0-85027948080&doi=10.1002%2f2014JB011176&partnerID=40&md5=29a7ce38c5cf3872d2276981d2f6b34f (cited By 326) doi: 10.1002/2014JB011176

Pfeffer, W. T., Arendt, A. A., Bliss, A., Bolch, T., Cogley, J. G., Gardner, A. S., … et al. (2014). The randolph glacier inventory: a globally complete inventory of glaciers. *Journal of Glaciology*, *60*(221), 537–552. doi: 10.3189/2014JoG13J176

Rajner, M. (2018). Detection of ice mass variation using gnss measurements at svalbard. *Journal of Geodynamics*, *121*, 20 - 25. Retrieved from http://www.sciencedirect.com/science/article/pii/S0264370718300450 doi: https://doi.org/10.1016/j.jog.2018.06.001

Root, B. C., Tarasov, L., & van der Wal, W. (2015). Grace gravity observations constrain weichselian ice thickness in the barents sea. *Geophysical Research Letters*, *42*(9), 3313-3320. Retrieved from https://agupubs.onlinelibrary.wiley.com/doi/abs/10.1002/2015GL063769 doi: 10.1002/2015GL063769

Sato, T., Okuno, J., Hinderer, J., MacMillan, D. S., Plag, H.-P., Francis, O., … Fukuda, Y. (2006, 06). A geophysical interpretation of the secular displacement and gravity rates observed at Ny-Ålesund, Svalbard in the Arctic—effects of post-glacial rebound and present-day ice melting. *Geophysical Journal International*, *165*(3), 729-743. Retrieved from https://doi.org/10.1111/j.1365-246X.2006.02992.x doi: 10.1111/j.1365-246X.2006.02992.x

Sørensen, L. S., Jarosch, A. H., Adalgeirsdóttir, G., Barletta, V. R., Forsberg, R., Pálsson, F., ... Jóhannesson, T. (2017, 01). The effect of signal leakage and glacial isostatic rebound on GRACE-derived ice mass changes in Iceland. *Geophysical Journal International*, *209*(1), 226-233. Retrieved from https://doi.org/10.1093/gji/ggx008 doi: 10.1093/gji/ggx008

Tushingham, A. M., & Peltier, W. R. (1991). Ice-3g: A new global model of late pleistocene deglaciation based upon geophysical predictions of post-glacial relative sea level change. *Journal of Geophysical Research: Solid Earth*, *96*(B3), 4497-4523. Retrieved from https://agupubs.onlinelibrary.wiley.com/doi/abs/10.1029/90JB01583 doi: 10.1029/90JB01583

VanLooy, J., Forster, R., & Ford, A. (2006). Accelerating thinning of kenai peninsula glaciers, alaska. *Geophysical Research Letters*, *33*(21). Retrieved from https://agupubs.onlinelibrary.wiley.com/doi/abs/10.1029/2006GL028060 doi: 10.1029/2006GL028060

Whitehouse, P. L., Allen, M. B., & Milne, G. A. (2007, 08). Glacial isostatic adjustment as a control on coastal processes: An example from the Siberian Arctic. *Geology*, *35*(8), 747-750. Retrieved from https://doi.org/10.1130/G23437A.1 doi: 10.1130/G23437A.1

Supporting Information for "Vertical Land Motion from present-day deglaciation in the wider Arctic"

Carsten Ankjær Ludwigsen[1], Shfaqat Abbas Khan[1], Ben Marzeion[2] and Ole Baltazar Andersen[1]

[1]DTU Space, Technical University of Denmark
[2]Institute of Geography and MARUM – Center for Marine Environmental Sciences, University of Bremen, Germany

Contents of this file

S1 Description of glacier ice model

As initial conditions, we use glacier outlines obtained from RGI 6.0 (Pfeffer et al., 2014). The time stamp of these outlines differs between glaciers, but is typically around the year 2000. To obtain results before this time, the model uses an iterative process to find the glacier geometry in the year of initialization (e.g., 1901) that results in the observed glacier geometry in the year of the outline's time stamp (e.g., 2000) after the model was run forward.

The model relies on monthly temperature and precipitation anomalies to calculate the specific mass balance of each glacier. Here, we use the mean of seven different reanalysis products as boundary conditions. Temperature is used to estimate the ablation of glaciers following a temperature-index melt model, and to estimate the solid fraction of total precipitation, which is used to estimate accumulation.

Mass balance data for each glacier is distributed over the glacier according to a mathematical approximation, assuming conservation of mass and that the glacier has a elevation gain at the top which becomes a elevation decline further down the glacier. The altitude where the elevation change goes from positive to negative, E, is approximated by a simple function of the glacial altitude (Z) and the averaged ice height change, ($\overline{\mathrm{h}} = \rho b A^{-1}$), and ρ is the ice density (917 kg m^{-3}). Note that E is different from the equilibrium line altitude (ELA).

$$\mathrm{E} = (1 - \bar{\mathrm{h}})\tilde{Z} \tag{S1}$$

where $\tilde{Z}$ is the median glacial height. For every glacier we define a distribution function, $D(i)$, where i represents a grid cell of the glacier:

$$D(i) = \quad 1 - \exp\left(\frac{(2-\bar{\mathrm{h}})(\mathrm{E}-Z(i))}{Z_{max}}\right) \tag{S2}$$

For all glaciers, is the elevation change assumed to be exponentially declining with height, $Z(i)$. The fraction in the exponential term makes sure that glaciers that on average gains up to 2 m height, will have an elevation loss in the bottom of the glacier and elevation gain at the top, unless E is equal or to Z_{max}, in which case, the whole glacier will be loosing height.

Corresponding author: Carsten Ankjær Ludwigsen, caanlu@space.dtu.dk

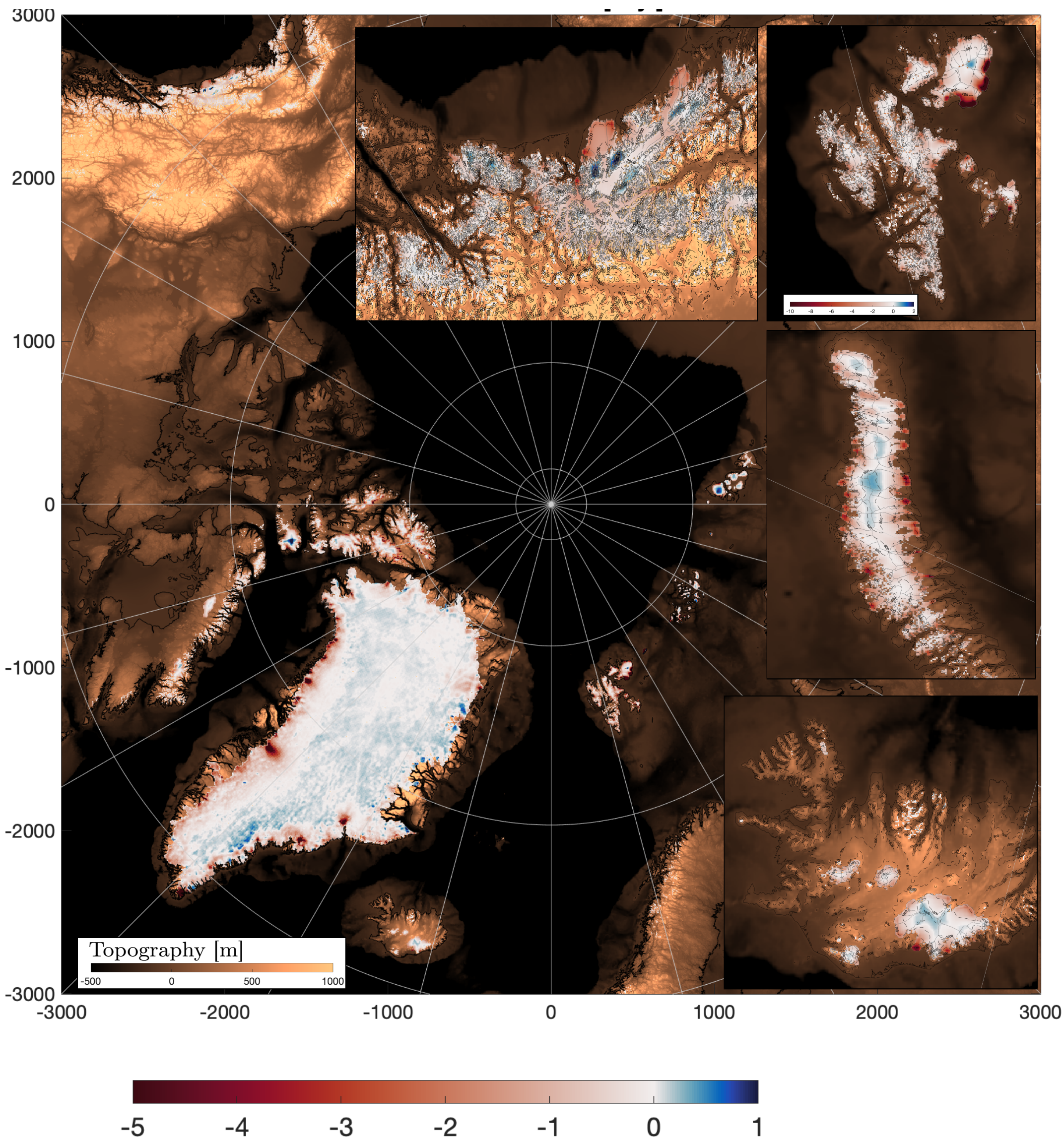

Figure S1.1. Ice elevation change from 2003 to 2015 in m yr^{-1} (red-blue scale) resulting from the redistribution explained above. The most interesting regions (Alaskian Coast, Svalbard (on a wider colorscale), Novaya Zemlja and Iceland) are enlarged. There is no significant ice loss in mainland Siberia.

The elevation change, dh/dt, is found by normalizing D, multiplying with the total mass balance, b, and converted to a height change by dividing with $\rho = 917$ kg m^{-3}.

$$\frac{dh(i)}{dt} = \frac{b}{\rho}\hat{D}(i) \qquad \text{where,} \tag{S3}$$

$$\hat{D}(i) = \frac{D(i)}{\sum_{i=1}^{k} D(i)} \tag{S4}$$

S1.1 Data availability

The ice model is available as a NetCDF-4 file on `ftp.space.dtu.dk/pub/DTU20/VLM`.

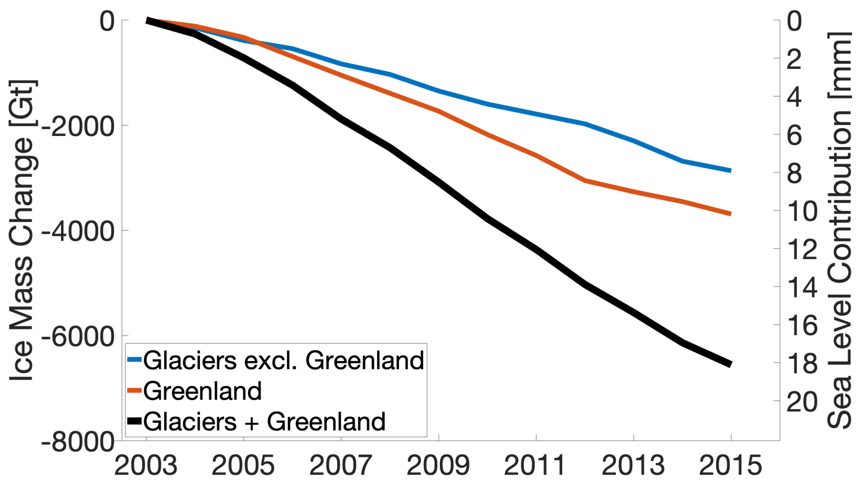

Figure S1.2. Ice loss from Greenland (including peripheral glaciers) and Arctic glaciers that goes in to the VLM calculations.

S2 Detailed description of the VLM signal at GNSS-site

In this section, we explain the VLM measured by GNSS in comparison to the VLM-model for the regions covered in this study.

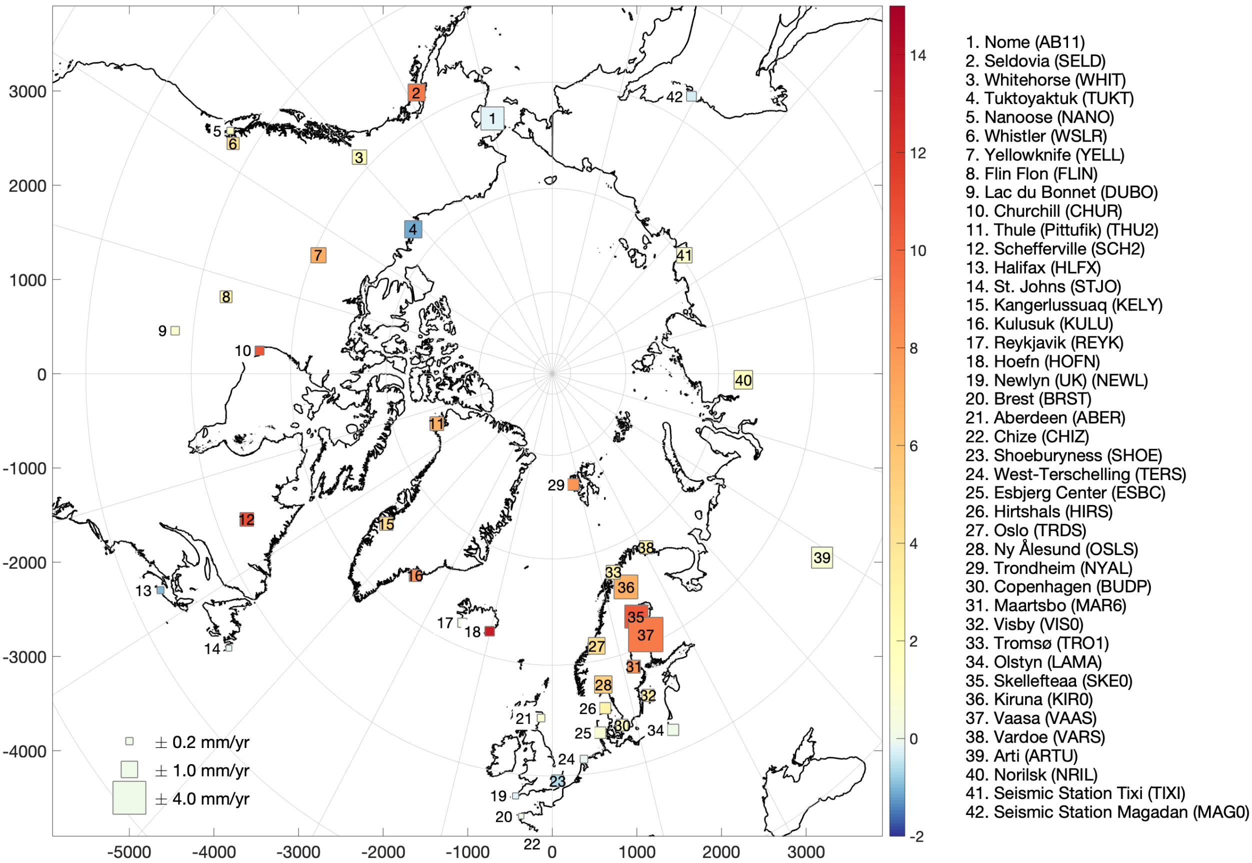

Figure S2.1. Location and name (and IGS abbreviation) of the 42 GNSS-sites used in this study ordered from most west to most east. The color indicates the linear trend from 2003-2015 [mm yr^{-1}], while the size of the square is proportional with the standard error (as estimated in the URL6-product).

S2.1 North America

The Alaskan GNSS stations show rates with opposite signs. Nome (AB11) in the Bering Strait, has a small elastic uplift which is countered by an sligthly larger GIA-caused subsidence. This results in a small total subsidence as it is also seen by the GNSS-site. Similar is the situation for Tuktoyaktuk (TUKT) where subsidience by GIA is -2.1 mm yr^{-1}, which results in a total VLM of -1.2 mm yr^{-1}, which matches the measured VLM.

The Alaska south coast which accounts for more than 25 % of the total glacial melt, is naturally dominated by elastic uplift, while GIA VLM is below 1 mm yr^{-1}. The GNSS-site Seldovia (SELD) shows large GNSS-measured uplift rates of 9.1 ± 1.1 mm yr^{-1}, while the elastic uplift rate is only 1.1 ± 0.6 mm yr^{-1} and GIA-rate -0.1 ± 0.8 mm yr^{-1}. In total this gives the second largest difference between the VLM model and GNSS VLM of the locations included in this study. Seldovia is located on the Kenai Peninsula close to the Kenai Fjords, which experienced an accelerated glacial Ice Loss in the 20th century (VanLooy et al., 2006). This is, however, not enough to explain the increased measured uplift. GIA-estimates vary in the region (Larsen et al., 2005; Hu & Freymueller, 2019), but is not more than around 1-2 mm yr^{-1}. A postseismic signal following the Prince

	IGS id	Abbr.	elastic VLM	GIA VLM	VLM-model	GNSS VLM	Model-GNSS
Nome	4	AB11	0.5 ± 0.1	-0.8 ± 0.3	-0.2 ± 0.5	-0.2 ± 2.0	-0.1 ± 2.0
Seldovia	517	SELD	1.1 ± 0.6	-0.1 ± 0.8	1.0 ± 1.3	9.1 ± 1.1	-8.2 ± 1.7
Whitehorse	651	WHIT	1.6 ± 0.8	0.9 ± 1.3	2.6 ± 2.1	2.1 ± 0.8	0.5 ± 2.2
Tuktoyaktuk	602	TUKT	0.9 ± 0.2	-2.1 ± 0.9	-1.2 ± 1.1	-1.1 ± 1.1	-0.1 ± 1.5
Nanoose	341	NANO	0.6 ± 0.3	1.5 ± 2.7	2.1 ± 3.0	1.5 ± 0.2	0.6 ± 3.0
Whistler	656	WSLR	0.9 ± 0.7	2.5 ± 3.1	3.4 ± 3.8	4.3 ± 0.5	-0.9 ± 3.8
Yellowknife	664	YELL	0.8 ± 0.2	7.6 ± 1.5	8.5 ± 1.7	6.9 ± 0.8	1.6 ± 1.9
Flin Flon	168	FLIN	0.6 ± 0.2	8.3 ± 1.6	8.9 ± 1.8	3.0 ± 0.5	5.9 ± 1.9
Lac du Bonnet	143	DUBO	0.6 ± 0.2	3.7 ± 1.1	4.3 ± 1.3	1.0 ± 0.3	3.3 ± 1.3
Churchill	106	CHUR	0.8 ± 0.3	8.4 ± 2.8	9.3 ± 3.1	10.6 ± 0.3	-1.3 ± 3.1
Thule (Pittufik)	583	THU2	5.9 ± 2.9	0.1 ± 2.1	6.0 ± 5.0	6.8 ± 0.7	-0.7 ± 5.1
Schefferville	510	SCH2	1.0 ± 0.3	15.7 ± 2.3	16.7 ± 2.6	11.0 ± 0.7	5.7 ± 2.7
Halifax	211	HLFX	0.5 ± 0.2	-1.5 ± 0.8	-1.0 ± 1.1	-1.0 ± 0.2	0.0 ± 1.1
St. Johns	548	STJO	0.7 ± 0.3	-1.4 ± 0.3	-0.7 ± 0.6	-0.1 ± 0.1	-0.5 ± 0.6
Kangerlussuaq	247	KELY	7.2 ± 3.3	2.9 ± 3.4	10.0 ± 6.6	4.7 ± 0.7	5.4 ± 6.7
Kulusuk	265	KULU	5.7 ± 1.8	-1.5 ± 1.0	4.3 ± 2.8	8.2 ± 0.5	-3.9 ± 2.9
Reykjavik	479	REYK	1.9 ± 0.5	0.2 ± 1.4	2.2 ± 2.0	0.0 ± 0.3	2.1 ± 2.0
Hoefn	215	HOFN	2.5 ± 1.0	-0.1 ± 1.0	2.3 ± 2.0	13.3 ± 0.3	-10.9 ± 2.0
Newlyn (UK)	347	NEWL	0.6 ± 0.2	-1.1 ± 0.2	-0.5 ± 0.4	-0.2 ± 0.1	-0.3 ± 0.4
Brest	72	BRST	0.5 ± 0.2	-1.0 ± 0.2	-0.5 ± 0.4	0.1 ± 0.1	-0.6 ± 0.4
Aberdeen	10	ABER	0.8 ± 0.2	-0.5 ± 0.4	0.3 ± 0.6	0.8 ± 0.2	-0.6 ± 0.7
Chize	102	CHIZ	0.4 ± 0.1	-0.3 ± 0.1	0.1 ± 0.3	0.0 ± 0.3	0.1 ± 0.4
Shoeburyness	531	SHOE	0.6 ± 0.2	-0.8 ± 0.4	-0.2 ± 0.6	-0.6 ± 0.5	0.4 ± 0.8
West-Terschelling	568	TERS	0.6 ± 0.2	-0.9 ± 0.7	-0.3 ± 0.9	-0.1 ± 0.2	-0.2 ± 0.9
Esbjerg Center	153	ESBC	0.6 ± 0.2	-0.1 ± 0.5	0.5 ± 0.7	0.8 ± 0.5	-0.2 ± 0.9
Hirtshals	210	HIRS	0.7 ± 0.2	2.2 ± 0.8	2.9 ± 1.0	2.9 ± 0.5	-0.0 ± 1.1
Oslo	596	OSLS	0.9 ± 0.2	4.6 ± 1.1	5.5 ± 1.4	4.3 ± 1.0	1.2 ± 1.7
Trondheim	370	TRDS	0.8 ± 0.2	5.0 ± 1.8	5.8 ± 2.0	5.3 ± 1.1	0.5 ± 2.3
Ny Ålesund	378	NYAL	4.9 ± 1.5	0.5 ± 0.4	5.4 ± 1.9	8.0 ± 0.5	-2.6 ± 2.0
Copenhagen	75	BUDP	0.6 ± 0.2	0.9 ± 0.5	1.5 ± 0.6	1.7 ± 0.5	-0.2 ± 0.8
Maartsbo	306	MAR6	0.7 ± 0.2	7.6 ± 2.4	8.3 ± 2.6	8.0 ± 0.6	0.3 ± 2.7
Visby	639	VIS0	0.6 ± 0.2	3.3 ± 1.1	3.9 ± 1.3	3.4 ± 0.6	0.5 ± 1.4
Tromsø	599	TRO1	1.0 ± 0.3	1.7 ± 0.7	2.7 ± 0.9	3.1 ± 0.7	-0.4 ± 1.2
Olstyn	274	LAMA	0.5 ± 0.1	0.1 ± 0.5	0.6 ± 0.7	0.0 ± 0.5	0.5 ± 0.8
Skellefteaa	534	SKE0	0.8 ± 0.2	8.5 ± 2.1	9.3 ± 2.3	10.4 ± 2.0	-1.0 ± 3.1
Kiruna	252	KIR0	0.9 ± 0.3	5.2 ± 0.9	6.1 ± 1.1	6.8 ± 2.1	-0.7 ± 2.4
Vaasa	625	VAAS	0.7 ± 0.2	8.3 ± 2.2	9.0 ± 2.4	9.1 ± 4.4	-0.1 ± 5.0
Vardoe	630	VARS	0.9 ± 0.3	2.0 ± 0.6	2.9 ± 0.8	3.1 ± 0.6	-0.1 ± 1.1
Arti	36	ARTU	0.2 ± 0.1	-0.2 ± 0.2	-0.0 ± 0.3	0.8 ± 1.6	-0.8 ± 1.7
Norilsk	360	NRIL	0.5 ± 0.2	1.9 ± 0.2	2.4 ± 0.4	1.8 ± 1.3	0.6 ± 1.3
Seismic Station Tixi	587	TIXI	0.5 ± 0.1	-0.3 ± 0.3	0.1 ± 0.4	1.0 ± 0.9	-0.9 ± 1.0
Seismic Station Magadan	298	MAG0	0.2 ± 0.1	-0.2 ± 0.2	-0.0 ± 0.2	-0.3 ± 0.3	0.3 ± 0.4

Table S2.1. Measured and modelled VLM for each GNSS-site in mm yr^{-1}. VLM-model is the sum of elastic VLM and GIA VLM.

Willam Sound Earthquake in 1964 explained by Cohen and Freymueller (2001) is still causing a locally increased uplift on this side of the peninsula. Our study indicate this effect to be 8.2 mm yr^{-1} from 2003-2015, which roughly matches the study by Cohen and Freymueller (2001), where they find the post seismic uplift to be 9.3 mm yr^{-1} from 1994-2001. This rebound is expected to decay further over time, but will still be relevant for decades to come (Cohen & Freymueller, 2001).

Whitehorse, Nanoose and Whistler, are dominated by large GIA-uncertainties, which are larger than the VLM-signal itself and 3-4 times larger than the residual between the VLM model and GNSS VLM. Yellowknife (YELL), Flin Flon (FLIN) and Lac du Bonnet (DUBO) are at the periphery of the largest GIA-rate, but have no large nearby glaciers to cause significant elastic uplifts. It is an area known to have uncertain GIA-estimates, e.g. does the ICE6G-model (Peltier et al., 2015) have lower GIA-rates in better alignment with the measured GNSS VLM. The same residuals are also seen by Frederikse et al. (2019), which uses the same GIA model (Caron2018). The VLM predictions for Churchill

(CHUR) at the south-east coast of Hudson Bay, is in good alignment with the GNSS-measured VLM, while the deformationen rate for Schefferville (SCH2) also is overestimated in the model.

At the Canadian Atlantic coast is GIA causing a subsidence. The VLM model shows, that a smaller positive elastic deformation is mitigating the subsidence, which in total gives a rate in the order of -1 mm yr^{-1}, which agrees well with GNSS VLM measured at Halifax, Nova Scotia (HLFX) and St. Johns, New Foundland (STJO).

S2.2 Iceland

The two GNSS-sites in this study show very different uplift rates of 0.0 ± 0.3 mm yr^{-1} in Reykjavik (REYK) and 13.3 ± 0.3 mm yr^{-1} at Hoefn (HOFN) at the southnern edge of the largest ice cap on Iceland, Vatnajökull. The VLM-model overestimates the rebound in Reykjavik while it largely underestimates it at Hoefn. A probable explanation for this is the thin crustal layer and a soft viscoelastic mantly layer (Fleming et al., 2007), which creates a present-day viscoelastic signal that is much larger than the ones predicted by the GIA-model or in the 1-D earth rheology included in the elastic VLM-calculations (Sørensen et al., 2017). A thin crust, also means that the uplift decreases faster with distance to the glacier (Fleming et al., 2007), which could explain why Reykjavik shows little vertical deformation.

S2.3 Svalbard

The majority of land in Svalbard is covered with ice, and vertical deformation highly influenced by ongoing ice-mass changes. The only site from Svalbard included in this study is Ny Ålesund (NYAL), which is located on the west coast. At this location, the VLM-model is dominated by an elastic uplift of 4.9 ± 1.5 mm yr^{-1} and GIA of 0.5 ± 0.4 mm yr^{-1}. In total this is 2.6 mm yr^{-1} short of the measured GNSS VLM. While global GIA-models agree within $\pm$ 0.2 mm yr^{-1}, more focused, but older studies predict a slightly higher GIA contribution of around 1.5 mm yr^{-1} (Sato et al., 2006; Kierulf et al., 2009). Another contribution to VLM, which is relevant for VLM-studies in glaciated regions, is the 'short-term mantle memory', (Mémin et al., 2014; Rajner, 2018), which is a non-instant relaxation of the mantle after being depressed by an load. Svalbard likely experienced significant deglaciation after the little ice age (LIA) that ended in the end of the 19th century (Grove, 2001). The effect is quite uncertain (Rajner, 2018) and Mémin et al. (2014) estimated the post-LIA rebound to be 2-5 mm yr^{-1} in the beginning of 21st century, which would explain the residual of 2.6 mm yr^{-1}.

S2.4 Northern Europe and Scandinavia

The fennoscandinavian icecap from the last ice ages is causing a GIA that is dominating the vertical deformation in Scandinavia (figure 1). Even though small glaciers exist in particular Norway, the elastic effect is very local and has almost negligible effect on the GNSS-sites in this study. The contour lines of the elastic rebound are clearly parallel to Greenland (figure 1), which indicates, that the wavelength of the elastic VLM of Greenland is determining the elastic VLM in Scandinavia and Northern Europe.

GIA is around 3-5 times larger than the elastic VLM in most of Scandinavia. However it is clear, that for many of the GNSS-sites, can the VLM-signal only be explained by combining the elastic VLM model with GIA. This becomes more prominent for GNSS-sites in areas, where GIA is less dominant. Esbjerg (ESBC) on the west coast of Denmark is close to the zero-line of the GIA VLM, but is still measuring an uplift of about 0.8 mm yr^{-1}. The VLM-model predicts elastic uplift rates of about 0.6 ± 0.2 mm yr^{-1}, which agrees with the GNSS VLM. South of the zero-line in Northern Europe, where the

GIA-rate is negative, the elastic VLM caused by present day ice melt, is somewhat mitigating the subsidence, which is also seen along the North American east coast.

S2.5 Siberia

Only a few available GNSS measurements exist in eastern Europe and Siberia. The GIA-model by Caron et al. (2018) is also challenged by limited resources of paleo sea-level records, which makes the GIA-model more dependent on the existing GNSS-records. It is commonly anticipated that Siberia had little or no ice during the last glacial cycle (Whitehouse et al., 2007), except some ice in the north central Siberia and in the shallow waters in the Barents Sea between Svalbard and Novaya Zemlya (Root et al., 2015). The old ICE3G GIA model by Tushingham and Peltier (1991) contained included some prehistoric ice over the western Siberia, which disappeared in the later version ICE5G and ICE6G (Peltier et al., 2015).

Also the Elastic uplift is limited in the region, with values around 0.5 mm yr^{-1}. While the GNSS VLM is within in the error-range of the modelled VLM for the Siberian GNSS-sites (Arti (ARTU), Norilsk (NRIL), Tixi (TIXI) and Magadan (MAG0)), it seems that a GIA-only model would better fit the GNSS measurements, which possibly is because of the enhanced GNSS-dependency of the GIA-model.

S3 Timeseries of vertical deformation at all GNSS sites

Figure S3.1 shows both measured and modeled vertical deformation from 2003-2015 of each individual GNSS-site. It also reflects, how elastic VLM is changing year by year, while GIA is linear.

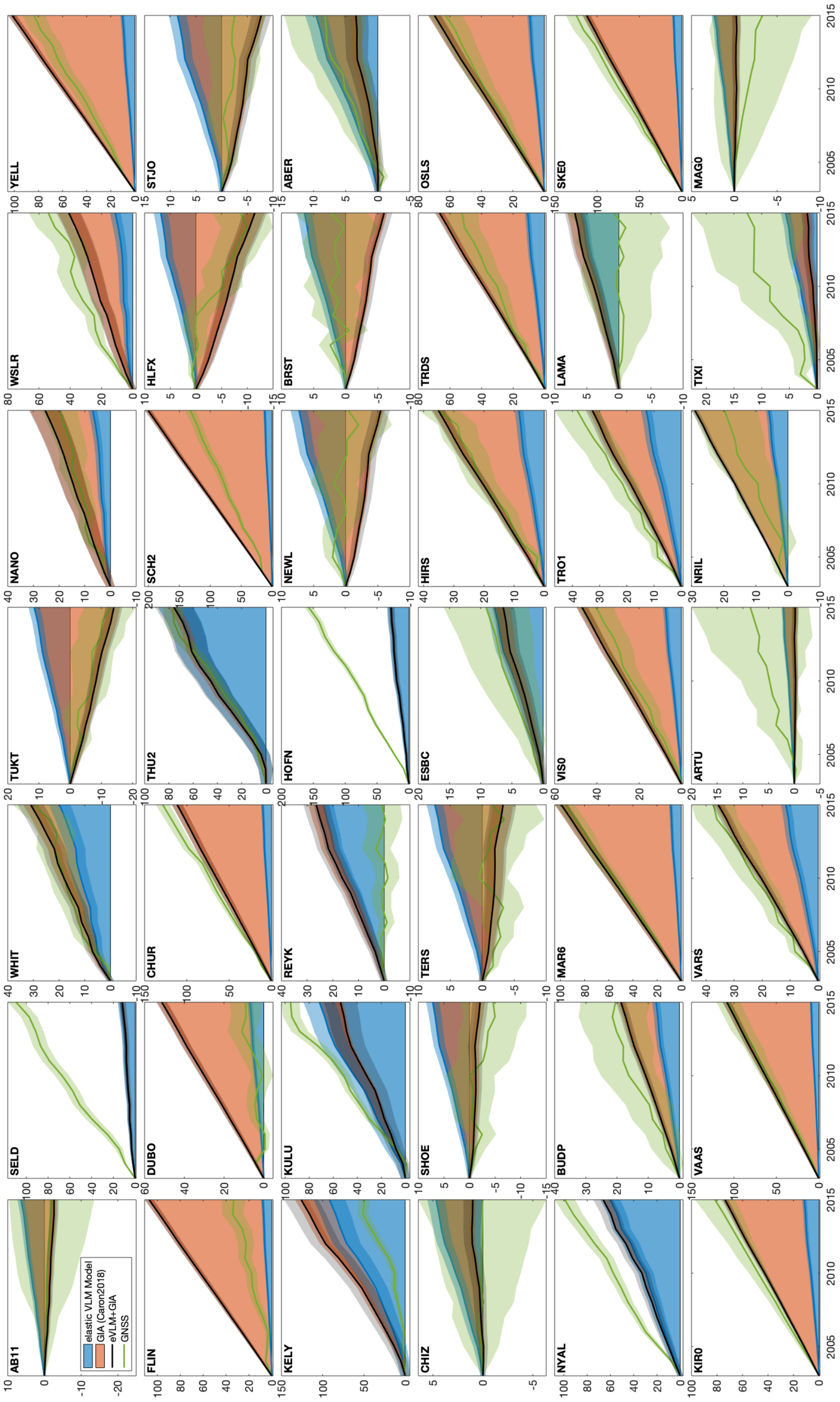

Figure S3.1. Measured and predicted vertical deformation from 2003 to 2015 for the 42 GNSS locations. GNSS is shown by the green line (green shadow denotes the error range) and the VLM model by the black line (error range is shown by the grey area). The red and blue areas indicate the part of the VLM model that is elastic and GIA.

References

Caron, L., Ivins, E. R., Larour, E., Adhikari, S., Nilsson, J., & Blewitt, G. (2018). Gia model statistics for grace hydrology, cryosphere, and ocean science. *Geophysical Research Letters*, *45*(5), 2203-2212. Retrieved from https://agupubs.onlinelibrary.wiley.com/doi/abs/10.1002/2017GL076644 doi: 10.1002/2017GL076644

Cohen, S. C., & Freymueller, J. T. (2001). Crustal uplift in the south central alaska subduction zone: New analysis and interpretation of tide gauge observations. *Journal of Geophysical Research: Solid Earth*, *106*(B6), 11259-11270. Retrieved from https://agupubs.onlinelibrary.wiley.com/doi/abs/10.1029/2000JB900419 doi: 10.1029/2000JB900419

Fleming, K., Martinec, Z., & Wolf, D. (2007, 01). Glacial-isostatic adjustment and the viscosity structure underlying the vatnajökull ice cap, iceland. *Pure and Applied Geophysics*, *164*, 751-768. doi: 10.1007/s00024-007-0187-6

Frederikse, T., Landerer, F. W., & Caron, L. (2019). The imprints of contemporary mass redistribution on local sea level and vertical land motion observations. *Solid Earth*, *10*(6), 1971–1987. Retrieved from https://www.solid-earth.net/10/1971/2019/ doi: 10.5194/se-10-1971-2019

Grove, J. (2001, 01). The initiation of the "little ice age" in regions round the north atlantic. *Climatic Change*, *48*, 53-82. doi: 10.1023/A:1005662822136

Hu, Y., & Freymueller, J. T. (2019). Geodetic observations of time-variable glacial isostatic adjustment in southeast alaska and its implications for earth rheology. *Journal of Geophysical Research: Solid Earth*, *124*(9), 9870-9889. Retrieved from https://agupubs.onlinelibrary.wiley.com/doi/abs/10.1029/2018JB017028 doi: 10.1029/2018JB017028

Kierulf, H. P., Plag, H.-P., & Kohler, J. (2009, 10). Surface deformation induced by present-day ice melting in Svalbard. *Geophysical Journal International*, *179*(1), 1-13. Retrieved from https://doi.org/10.1111/j.1365-246X.2009.04322.x doi: 10.1111/j.1365-246X.2009.04322.x

Larsen, C. F., Motyka, R. J., Freymueller, J. T., Echelmeyer, K. A., & Ivins, E. R. (2005). Rapid viscoelastic uplift in southeast alaska caused by post-little ice age glacial retreat. *Earth and Planetary Science Letters*, *237*(3), 548 - 560. Retrieved from http://www.sciencedirect.com/science/article/pii/S0012821X05004152 doi: https://doi.org/10.1016/j.epsl.2005.06.032

Mémin, A., Spada, G., Boy, J.-P., Rogister, Y., & Hinderer, J. (2014, 05). Decadal geodetic variations in Ny-Ålesund (Svalbard): role of past and present ice-mass changes . *Geophysical Journal International*, *198*(1), 285-297. Retrieved from https://doi.org/10.1093/gji/ggu134 doi: 10.1093/gji/ggu134

Peltier, W., Argus, D., & Drummond, R. (2015). Space geodesy constrains ice age terminal deglaciation: The global ice-6g-c (vm5a) model. *Journal of Geophysical Research: Solid Earth*, *120*(1), 450-487. Retrieved from https://www.scopus.com/inward/record.uri?eid=2-s2.0-85027948080&doi=10.1002%2f2014JB011176&partnerID=40&md5=29a7ce38c5cf3872d2276981d2f6b34f (cited By 326) doi: 10.1002/2014JB011176

Pfeffer, W. T., Arendt, A. A., Bliss, A., Bolch, T., Cogley, J. G., Gardner, A. S., … et al. (2014). The randolph glacier inventory: a globally complete inventory of glaciers. *Journal of Glaciology*, *60*(221), 537–552. doi: 10.3189/2014JoG13J176

Rajner, M. (2018). Detection of ice mass variation using gnss measurements at svalbard. *Journal of Geodynamics*, *121*, 20 - 25. Retrieved from http://www.sciencedirect.com/science/article/pii/S0264370718300450 doi: https://doi.org/10.1016/j.jog.2018.06.001

Root, B. C., Tarasov, L., & van der Wal, W. (2015). Grace gravity observations constrain weichselian ice thickness in the barents sea. *Geophysical Research Letters*, *42*(9), 3313-3320. Retrieved from https://agupubs.onlinelibrary

.wiley.com/doi/abs/10.1002/2015GL063769 doi: 10.1002/2015GL063769

Sato, T., Okuno, J., Hinderer, J., MacMillan, D. S., Plag, H.-P., Francis, O., ... Fukuda, Y. (2006, 06). A geophysical interpretation of the secular displacement and gravity rates observed at Ny-Ålesund, Svalbard in the Arctic—effects of post-glacial rebound and present-day ice melting. *Geophysical Journal International*, *165*(3), 729-743. Retrieved from https://doi.org/10.1111/j.1365-246X.2006.02992.x doi: 10.1111/j.1365-246X.2006.02992.x

Sørensen, L. S., Jarosch, A. H., Adalgeirsdóttir, G., Barletta, V. R., Forsberg, R., Pálsson, F., ... Jóhannesson, T. (2017, 01). The effect of signal leakage and glacial isostatic rebound on GRACE-derived ice mass changes in Iceland. *Geophysical Journal International*, *209*(1), 226-233. Retrieved from https://doi.org/10.1093/gji/ggx008 doi: 10.1093/gji/ggx008

Tushingham, A. M., & Peltier, W. R. (1991). Ice-3g: A new global model of late pleistocene deglaciation based upon geophysical predictions of post-glacial relative sea level change. *Journal of Geophysical Research: Solid Earth*, *96*(B3), 4497-4523. Retrieved from https://agupubs.onlinelibrary.wiley.com/doi/abs/10.1029/90JB01583 doi: 10.1029/90JB01583

VanLooy, J., Forster, R., & Ford, A. (2006). Accelerating thinning of kenai peninsula glaciers, alaska. *Geophysical Research Letters*, *33*(21). Retrieved from https://agupubs.onlinelibrary.wiley.com/doi/abs/10.1029/2006GL028060 doi: 10.1029/2006GL028060

Whitehouse, P. L., Allen, M. B., & Milne, G. A. (2007, 08). Glacial isostatic adjustment as a control on coastal processes: An example from the Siberian Arctic. *Geology*, *35*(8), 747-750. Retrieved from https://doi.org/10.1130/G23437A.1 doi: 10.1130/G23437A.1